J Solid State Electrochem (2010) 14:1769–1775
DOI 10.1007/s10008-010-1054-4

ORIGINAL PAPER

Enhancement of electrochemical properties of MoO_3 nanobelts electrode using PEG as surfactant for lithium battery

Varishetty Madhu Mohan · Hu Bin · Wen Chen

Received: 22 November 2009 / Revised: 5 March 2010 / Accepted: 16 March 2010 / Published online: 15 April 2010

Abstract Molybdenum trioxide (MoO_3) has attracted considerable attention due to their typical two-dimensional layered structure consisting of double layers of edge- and vertex-sharing MoO_6 octahedral being weakly held together by van der Waals bonds. These MoO_3 nanostructures and their polymer composites are currently drawing interest for the potential applications of Li batteries, supercapacitors, and other electrochemical as well as electrochromic display devices. In this paper, we report the synthesis of MoO_3 nanobelts and polyethylene glycol (PEG) surfactant MoO_3 nanobelts by hydrothermal method. Structure and morphology of the samples were investigated by X-ray diffraction, Fourier transform spectroscopy, scanning electron microscopy, and transmission electron microscopy (TEM). The pure MoO_3 nanobelts show an initial specific capacity of 275 mAh g^{-1}, whereas the 0.5 mol% PEG surfactant MoO_3 nanobelts show 307 mAh g^{-1} at constant current density of 30.7 mA g^{-1} with the 1.0–3.0 V vs. Li/Li^+ potential range. It was found that PEG surfactant MoO_3 nanobelts show not only a high initial specific capacity but also show better cyclic performance compared with that of pure MoO_3 nanobelts. The PEG surfactant MoO_3 nanobelts show stability and improvement of the specific capacity due to decreasing the length, width, and thickness of the nanobelts by surface reaction. Electrochemical impedance spectroscopy reveals that the PEG surfactant MoO_3 nanobelts exhibit low electrode resistance compared with pure MoO_3 nanobelts.

V. Madhu Mohan · H. Bin · W. Chen (✉)
State Key Laboratory of Advanced Technology for Materials Synthesis and Processing, and School of Materials Science and Engineering, Wuhan University of Technology, Wuhan 430070, People's Republic of China
e-mail: chenw@whut.edu.cn

Keywords Hydrothermal method · MoO_3 nanobelts · Poly(ethylene glycol) · Cathode material · Electrochemical properties

Introduction

In recent years, conducting polymeric nanocomposites have attracted much attention because of their unique and novel properties and a wide variety of potential applications [1]. Nanobelts or nanoribbons, particularly semiconducting materials, have recently attracted considerable attention as a new group of quasi-one-dimensional (1D) nanostructures owing to their special characteristics, which differ from those of nanowires and nanotubes [2, 3]. The single crystalline nature and in particular their large aspect ratio as well as the faceting nature of these nanobelts make them ideal candidates for probing size-and dimensionality-dependent physical or chemical phenomena for applications of nanodevices [4]. Advances in the chemistry of insertion materials have been very important for the development of rechargeable lithium batteries, allowing the obtainment of electrodes with a high energy density and specific capacity. Some of the host matrices consist of transition metal oxides that enable easy access of lithium ions into their network [5]. A material of particular interest is MoO_3, which is a layered n-type semiconductor with various advanced applications as catalysts [6], gas sensors [7], batteries [8], lubricants [9], memory materials [10], and electrochromic devices [11, 12]. Hence, molybdenum oxide in the form of micro- and nanostructures are promising candidates for electronic and optoelectronic microdevices.

To date, various preparation methods of nanostructured MoO_x and their corresponding electrochemical performance have been reported. Among these methods are α-MoO_3

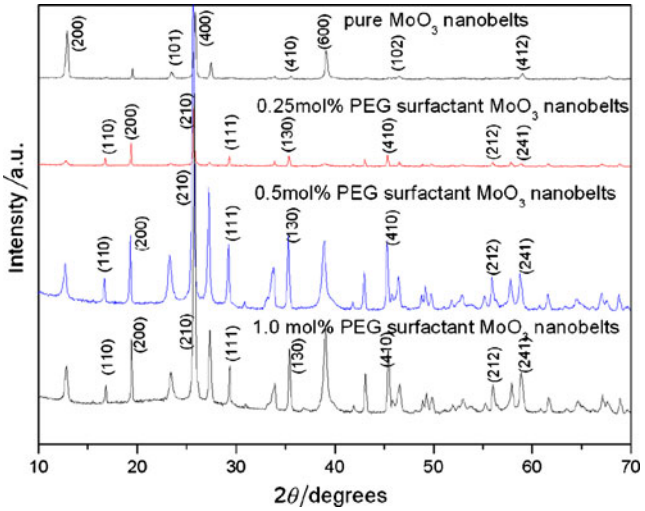

Fig. 1 X-ray diffraction patterns of MoO_3 nanobelts and PEG surfactant MoO_3 nanobelts

micro-rods by vapor-transportation method [13], the carbon/MoO_2 composite using tri-block copolymer as a structure directing agent and carbon source [14], MoO_3 nanobelts by hydrothermal reaction [15], utilizing poly(ethylene glycol) (PEG) [16], MoO_3 nanoparticles by hot-wire chemical vapor deposition [17, 18], tremella-like MoO_2 by hydrothermal reduction [19], the fissile MoO_2 by hydrothermal reaction [20, 21], the porous spherical MoO_2 by rheological phase reaction [21], MoO_2 by reduction of MoO_3 with ethanol vapor [22], etc. Comparatively less attention has been focused on solution-based chemical routes to oxide nanobelts through reactions in solution, which have the advantage of better uniformity and instrumental simplicity [4, 23, 24].

In this work, we report the synthesis of molybdenum trioxide nanobelts by a simple hydrothermal method. The morphology of MoO_3 nanobelts is affected with the addition of PEG. It is expected that the layered structures can also form this kind of belt-like morphology if the reaction conditions are properly controlled, which opens up opportunities for both fundamental studies and nanodevice application of lithium batteries.

Experimental

Synthesis of PEG surfactant MoO_3 nanobelts

First, MoO_3 nanobelts were synthesized by simple hydrothermal method without using any surfactant. The MoO_3 sols were prepared by the ion exchange of $(NH_4)_6Mo_7O_{24}{\cdot}4H_2O$ (≥99.0%) through a proton exchange resin, and the clear light-blue MoO_3 sols (final pH ~2.0) were obtained. Then, PEG was added to MoO_3 sols in the proportion of $(PEG)_xMoO_3$ (x=0, 0.25, 0.5, 1.0) to form the mixed sols. Finally, the mixed sols were directly added into a Teflon-lined autoclave and kept at 180°C for 48 h. After the hydrothermal reaction, the samples were washed with distilled water and ethanol then dried at 80°C for 12 h. It is worthy to note that the color of pure MoO_3 nanomaterials is light blue, and that of PEG surfactant MoO_3 nanomaterials becomes dark blue because Mo^{6+} ions are partially reduced to Mo^{5+} to form PEG surfactant MoO_3 nanobelts [25].

Preparation of Li batteries

Electrochemical batteries were assembled in a dry glove box filled with an argon gas using lithium pellets as negative electrode, 1 M solution of $LiPF_6$ in ethylene carbon/dimethyl carbonate as electrolyte and pellets made from the obtained products, and acetylene black and PTFE in a 6:4:1 ratio as the positive electrode.

Characterization

The X-ray powder diffraction (XRD) measurement was performed on a D/MAX-III X-ray diffractrometer with Cu–Kα (λ=1.5418 Å) radiation and graphite monochromator. Fourier-transform infrared (FTIR) absorption spectra were recorded using a 60-SXB IR spectrometer with a resolution of 4 cm^{-1}. The measurements were taken over a wave number range of 400–4,000 cm^{-1}. Scanning electron microscopy (SEM) images were obtained using a JSM-5610LV scanning electron microscope at 20 kV. Transmission electron microscopy (TEM) images were taken in a JEOL JEM-2010 FEF microscope operated at 200 kV. Cyclic voltammograms were measured with a scan rate of 0.5 mV s^{-1} at 1.5–3.5 V vs. Li/Li^+ potential range, and electrochemical impedance

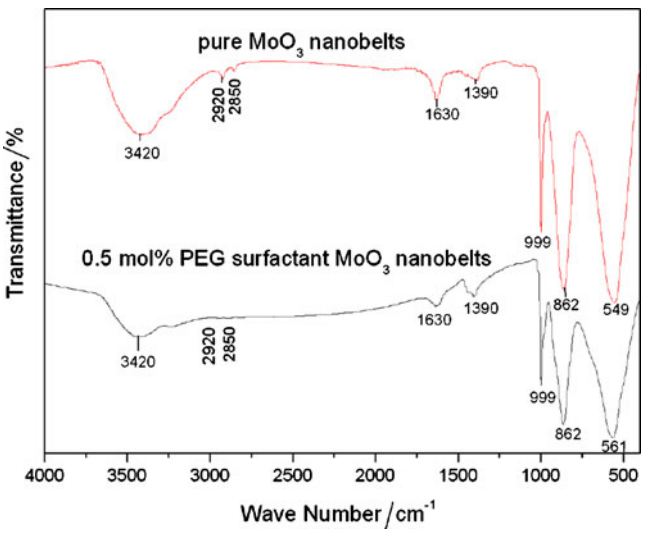

Fig. 2 FTIR spectra of MoO_3 nanobelts and 0.5 mol% PEG surfactant MoO_3 nanobelts

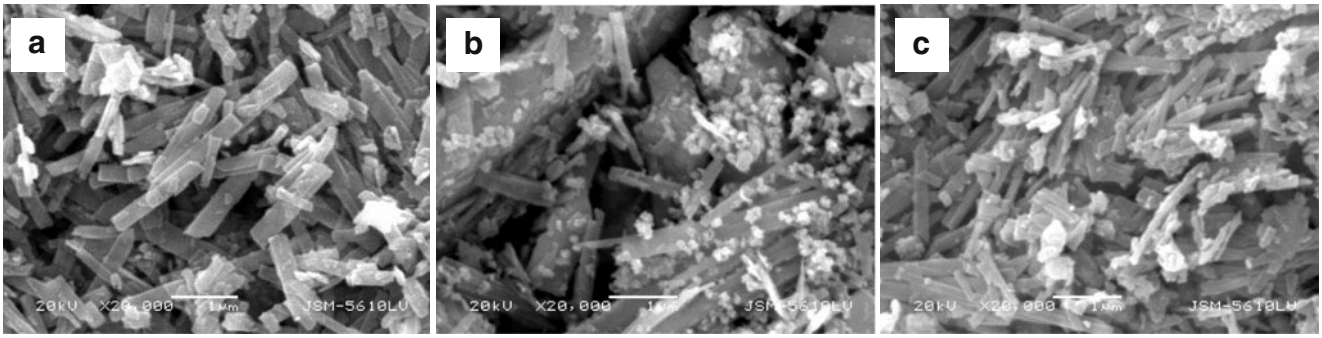

Fig. 3 SEM images of **a** MoO_3 nanobelts, **b** 0.25 mol% PEG surfactant MoO_3 nanobelts, and **c** 0.5 mol% PEG surfactant MoO_3 nanobelts

spectroscopy was investigated at different potentials by Autolab (Eco Chemie) model PGATAT30 (GPES/FRA) system. The discharge characteristics were analyzed by Battery Testing System (BTS-5V/5mA) which operated at a constant current density of 30.7 mA g^{-1} with 1.0–3.0 V vs. Li/Li^+ potential range.

Results and discussion

X-ray diffraction

Figure 1 shows the X-ray diffraction patterns of pure MoO_3 nanobelts and different mol% PEG surfactant MoO_3 nanobelts. From the XRD patterns, the phase composition of the pure MoO_3 and PEG surfactant MoO_3 nanobelts were identified as hexagonal space (JCPDS 05-0508). The 0.25, 0.5, and 1.0 mol% PEG surfactant MoO_3 nanobelts show the same structure with small changes to its lattice distances. This is due to less or high growth of nanobelts in the presence of PEG during the hydrothermal synthesis process.

FTIR spectra analysis

The FTIR spectra of the MoO_3 nanobelts and PEG surfactant MoO_3 nanobelts are shown in Fig. 2. The MoO_3 nanobelts exhibit three main vibrational modes in the range of 400–1,000 cm^{-1}. The terminal oxygen symmetry stretching mode (ν_s) of Mo=O and the bridge oxygen asymmetry and symmetry starching modes (ν_{as} and ν_s) of Mo–O–Mo are at 999, 862, and 549 cm^{-1}, respectively [15]. The O–H absorption bands appeared at 3,420 and 1,630 cm^{-1} which could be assigned due to the presence of water molecules. There are no PEG vibrational bands that appeared in the PEG surfactant MoO_3 nanobelts, which indicates that, after hydrothermal reaction, PEG content mostly decreased by washing.

SEM analysis

Figure 3 shows the SEM images of pure MoO_3 nanobelts and 0.25 mol%, 0.5 mol% PEG surfactant MoO_3 nanobelts. Pure MoO_3 nanobelts around 150–320 nm were grown individually and separately, whereas 0.25 mol%, 0.5 mol% PEG surfactant MoO_3 nanobelts were grown in the same way as pure MoO_3 nanobelts with lower length, width, and thickness due to high reactivity of PEG. The widths of the 0.25 mol%, 0.5 mol% PEG surfactant MoO_3 nanobelts were found to be 70–210 and 70–180 nm, respectively.

TEM analysis

Figure 4 shows the TEM images of pure MoO_3 nanobelts and 0.5 mol% PEG surfactant MoO_3 nanobelts. From Fig. 4a–b,

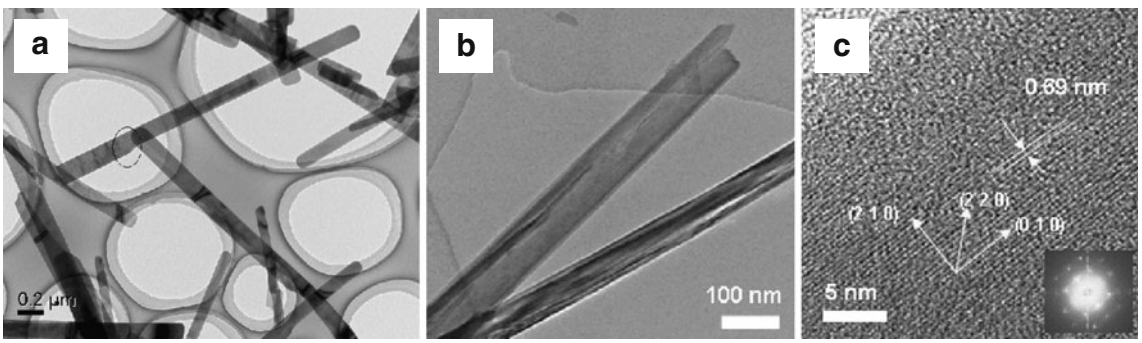

Fig. 4 TEM images of **a** MoO_3 nanobelts and **b–c** 0.5 mol% PEG surfactant MoO_3 nanobelts

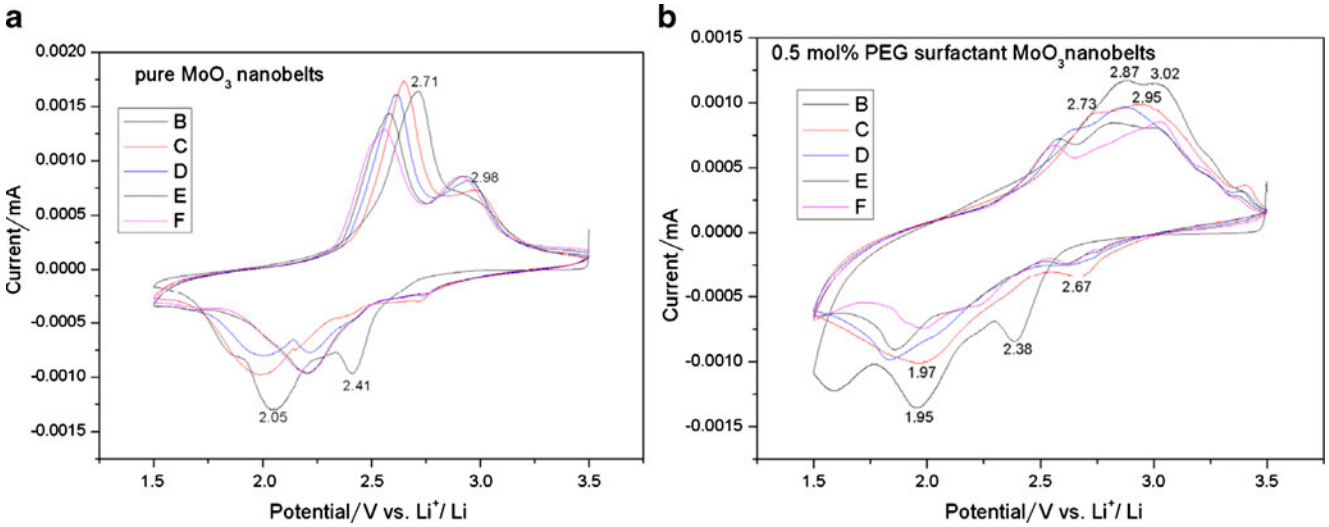

Fig. 5 Cyclic voltammograms of **a** MoO_3 nanobelts and **b** 0.5 mol% PEG surfactant MoO_3 nanobelts for the first five cycles

the breadth of MoO_3 nanobelts and 0.5 mol% PEG surfactant MoO_3 nanobelts were found to be 200 and 100 nm, respectively. From Fig. 4c, the lattice distance of the PEG surfactant MoO_3 nanobelts was found to be 0.69 nm which corresponds to the value of (210).

CV analysis

Figure 5 shows the first five cyclic voltammogram (CV) curves of pure MoO_3 nanobelts and PEG surfactant MoO_3 nanobelts. Cyclic voltammetry is one of the promising electroanalytical techniques for studying phase transformation of redox couple especially during the insertion and extraction process [26]. The area A_i (i=cycle times) which is surrounded by each cycle curve represents the amount of the Li^+ ion insertion. The cycle efficiency was calculated by the following equation:

$$Q_i = A_i/A_1 \quad (1)$$

where Q_i is the cycle efficiency, A_1 the area of the first cycle curve, and A_i the area of the i cycle curve. The third cycle efficiency of the Q_3 for pure MoO_3 and PEG surfactant MoO_3 nanobelts are found to be 85.96% and 89.36%, respectively. The higher cycle efficiency of PEG surfactant MoO_3 nanobelts indicates that the stability of cycling property increases when PEG is added to the MoO_3 nanobelts during the hydrothermal process. In addition, there are cathodic and anodic current peaks appearing at around the potentials of 2.05, 2.71 V and 2.41, 2.98 V in the first cycle of the pure MoO_3 nanobelts as shown in Fig. 5a. These two sets of peaks can be assigned to the insertion/extraction of Li^+ ions between the MoO_6 octahedron interlayers and intralayers [27]. It was found that the oxidation peaks shifted to certain potentials owing to the structure transformation and collapse of the active material [28]. This behavior was mostly observed in the case of MoO_3 nanobelts compared to that of PEG surfactant MoO_3 nanobelts, indicating that the cyclability of Li^+ ion insertion/extraction is decreased after several sweeps. Similar types of results were also observed in PEO/MoO_3 nanobelts and CX–SiO composites [26, 28].

Battery discharge characteristics

Figure 6 shows the discharge characteristics of pure MoO_3 and PEG surfactant MoO_3 nanobelts at different ratios with a 30.7 mA g^{-1} charge–discharge current density at 25 °C. The initial specific capacity of pure MoO_3 nanobelt is 276 mAh g^{-1}, but it sharply depreciated at the second cycle 200 $mAhg^{-1}$ probably due to the irreversible changes (such

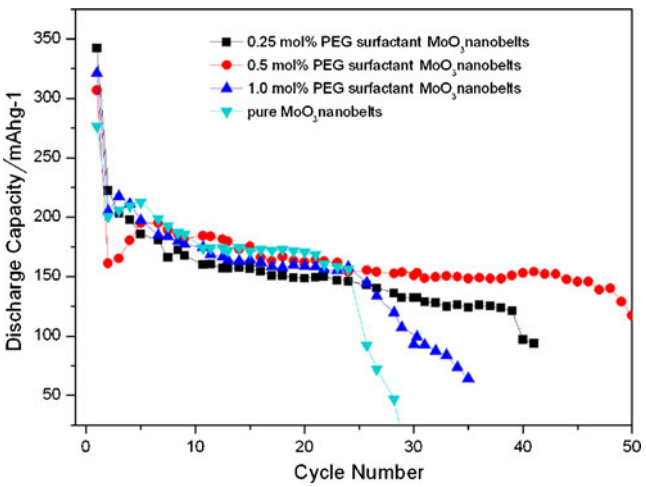

Fig. 6 The discharge characteristic curves of MoO_3 nanobelts and PEG surfactant MoO_3 nanobelts at different mol%

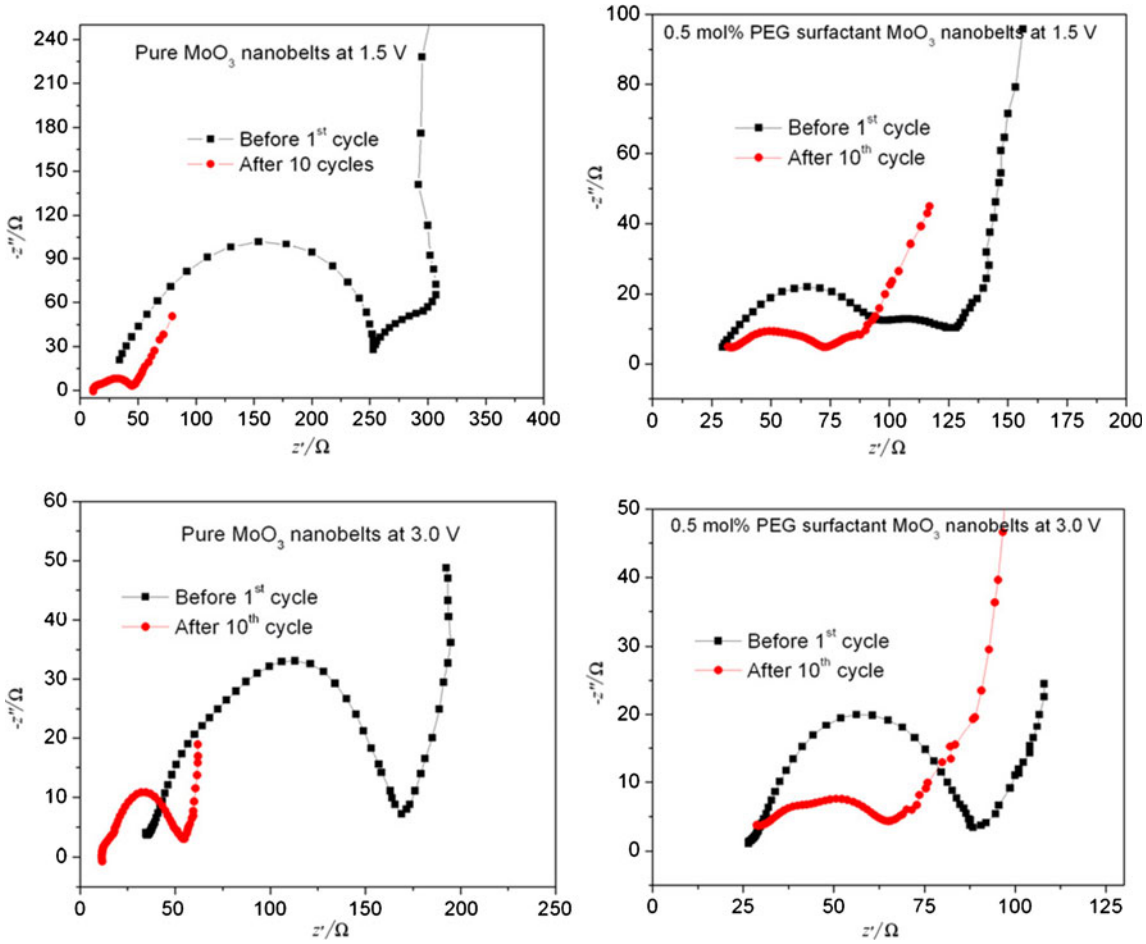

Fig. 7 Nyquist plots (Z' vs. $-Z''$) of MoO_3 nanobelts and 0.5 mol% PEG surfactant nanobelts at various potentials of 1.5 and 3.0 V

as crystallization) of the material's structure after the first lithium ion insertion/extraction process and/or some of the active sites of the electroactive material occupied by the lithium ions. The specific capacity increasing in the third cycle of pure MoO_3 nanobelts compared to that of the second cycle is likely due to the film cracking caused by the second cycle. The cracking or defects in the films after the second cycle allows more freedom for volumetric charge during Li^+ ion insertion/extraction [29]. After 25 cycles, the specific capacity of pure MoO_3 nanobelt battery abruptly decreased to 92 mAh g^{-1}, whereas the specific capacity of PEG surfactant MoO_3 nanobelts of 156 mAh g^{-1} indicates that the stability of the surfactant material battery increased. The discharge stability of the PEG surfactant MoO_3 nanobelts increases compared to that of pure MoO_3 nanobelts because the PEG decreased the length, width, and thickness of the nanobelts, which enhances the cyclic stability and reversibility due to the increase in the insertion/extraction of Li^+ ions. From these discharge characteristics, 0.5 mol% PEG surfactant MoO_3 nanobelts are one of the better possible candidates for lithium battery applications.

Electrochemical impedance spectroscopy

Electrochemical impedance spectroscopy (EIS) is a well-established technique to study electrode kinetics of cathode and anode materials [30]. EIS can give information about the surface film, charge transfer and bulk resistances of the electrode, the associated capacitances, and their variation in the applied voltage during the charge–discharge cycle [31]. Impedance plots obtained for PEG surfactant MoO_3 and

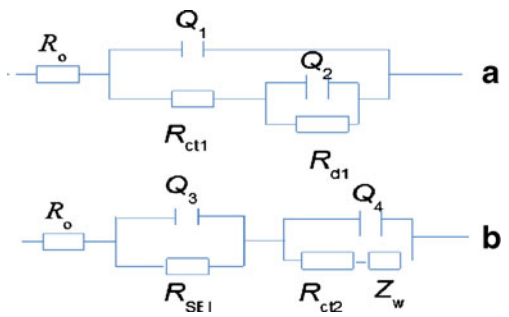

Fig. 8 Equivalent circuits for electrochemical impedance plots of **a** pure MoO_3 nanobelts and **b** PEG surfactant MoO_3 nanobelts batteries at 1.5 and 3.0 V potentials

pure MoO_3 nanobelts electrode batteries (1.5 and 3.0 V) are shown in Fig. 7. First, the presence of a semi-circular loop at higher frequencies is attributed to faradic reactions. The measured resistance (intercept of semicircle along the *x*-axis) is composed of the ionic resistance of electrolyte, the intrinsic resistance of the active material, and the contact resistance at the active material/current collector interface. Second, in the intermediate frequency region, the 45° line is the characteristic of ion diffusion into the porous structure of the electrode. Third, in the low frequency region, the slope of the impedance plot increases and tends to become purely capacitive (vertical line characteristic of a limiting diffusion process) which demonstrates that the electrochemical capacitance of the material was higher [32, 33]. As shown in Fig. 7, PEG surfactant nanobelts show much lower resistance in the higher frequency region, indicating better electronic conductivity, and smaller contact resistance between the materials or material and current collector compared to that of pure MoO_3 nanobelts. The probable reason is that PEG surfactant nanobelts have a much better contact area between the materials, which improves the electrical conductivity [34]. The equivalent circuit, which best fits the experimental data in the potential range 1.5 and 3.0 V for MoO_3 nanobelts as shown in Fig. 8a, can be expressed as

$$R_0(Q_1[R_{ct1}(R_{d1}Q_2)]) \quad (2)$$

where R_0 is the ohmic resistance of electrode and electrolyte, Q_1 and Q_2 are the constant phase elements, R_{ct1} is the charge transfer resistance of Faradic process occurring at the oxide/electrolyte interface, and R_{d1} is the ionic resistance arising from the diffusion of lithium ions. It was found that the potentials of 1.5 and 3.0 V for PEG surfactant MoO_3 nanobelts exhibit two partially overlapped semi-circles at the high-to-medium frequencies and a strait sloping line at low frequency [35].

The equivalent circuit for this cell system is depicted in Fig. 8b, where Q_3 and R_{SEI} are the capacitance and resistance of the solid electrolyte interface (SEI) corresponding to the semi-circle at high frequency, Q_4 and R_{ct2} (the double-layer capacitance and charge transfer resistance, respectively) correspond to the semi-circle at medium frequency, and Z_w (the Warburg impedance) corresponds to a strait sloping line at low frequency [36, 37]. It was observed that the diameter of the semi-circle at higher and medium frequencies depends on the transfer rate of Li^+ ions.

Conclusions

In the present paper, 1D MoO_3 nanobelts and PEG surfactant MoO_3 nanobelts were successfully synthesized using a simple hydrothermal method. There is no change in structure even after the addition of surfactant with different mol% of PEG to the MoO_3 nanobelts. The PEG surfactant MoO_3 nanobelts seem to have a higher specific capacity at the fifth cycle (82.6%) compared to that of pure MoO_3 nanobelts (78.9%). The 0.5 mol% PEG surfactant MoO_3 nanobelts show better stabilized specific capacity (156 mAh g^{-1}) at the 25th cycle which is higher than pure MoO_3 nanobelts (92 mAh g^{-1}). The PEG surfactant MoO_3 nanobelts exhibited less electrical resistance compared to pure MoO_3 nanobelts.

Acknowledgments One of the authors (Varishetty Madhu Mohan) wishes to thank the Wuhan University of Technology Management for the financial support in the form of Post-Doctoral Fellowship to carry out the above work. This work is supported by China Postdoctoral Science Foundation (CPSF; No. 20080440966), National Nature Science Foundation of China (No. 50672071, A3 Foresight Program-50821140308), and the Program for Changjiang Scholars and Innovative Research Team in University, Ministry of Education, China (PCSIRT) (No. IRT0547).

References

1. Petkov V, Parvanov V, Trikalitis P, Mallikas C, Vogt T, Kanatzidis MG (2005) J Am Chem Soc 127:8805
2. Law M, Sirbuly DJ, Johnson JC, Goldberger J, Saykally RJ, Yang P (2004) Science 305:1269
3. Li YB, Bando Y, Golberg D, Kurashima K (2002) Appl Phys Lett 81:5048
4. Wang S, Zhang Y, Ma X, Wang W, Li X, Zhang Z, Qian Y (2005) Solid State Commun 136:283
5. Huguenin F, Torresi RM (2008) J Phys Chem C 112:2202
6. Ponzi M, Duschatzky C, Carrascull A, Ponzi E (1998) Appl Catal A 169:373
7. Taurino AM, Forleo A, Francioso L, Siciliano P, Stalder M, Nesper R (2006) Appl Phys Lett 88:15211
8. Jung YS, Lee S, Ahn D, Dillon AC, Lee SH (2009) J Power Sources 188:286
9. Wang J, Rose KC, Lieber CM (1999) J Phys Chem B 103:8405
10. Ohta T, Takenaga M, Akahira N, Yamashita T (1982) J Appl Phys 53:8497
11. Jin A, Chen W, Zhu Q, Yang Y, Volkov VL, Zakharova GS (2009) Thin Solid Films 517:2023
12. Granqvist CG (1995) Handbook of inorganic electrochromic materials. Elsevier, Amsterdam
13. Li W, Cheng F, Tao Z, Chen J (2006) J Phys Chem B 110:119
14. Ji X, Subramanya P, Rho Y, Nazar LF (2007) Chem Mater 19:374
15. Mai L, Hu B, Chen W, Qi Y, Lao C, Yang R, Dai Y, Wang ZL (2007) Adv Mater 19:3712
16. Subba Reddy ChV, Walker EH Jr, Wen Chen, Sun-il Mho (2008) J Power Sources 183:330
17. Dillon AC, Mahan AH, Deshpande R, Parilla PA, Jones KM, Lee S (2008) Thin Solid Films 516:794
18. Lee SH, Kim YH, Deshpande R, Parilla PA, Whitney E, Gillaspie DT, Jones KM, Muhan AH, Zhang S, Dillon AC (2008) Adv Mater 20:3627
19. Yang LC, Gao QS, Zhang YH, Tang Y, Wu YP (2008) Electrochem Commun 10:118
20. Liang Y, Yang S, Yi Z, Lei X, Sun J, Zhou Y (2005) Mater Sci Eng B 121:152

21. Liang Y, Yang S, Yi Z, Sun J, Zhou Y (2005) Mater Chem Phys 93:395
22. Yang LC, Gao QS, Tang Y, Wu YP, Holze R (2008) J Power Sources 179:357
23. Zhang L, Yu JC, Xu AW, Li Q, Kwong KW, Wu L (2003) Chem Commun 23:2910
24. Wang JW, Li YD (2003) Chem Commun 18:2320
25. Qi YY, Chen W, Mai LQ, Zhu QY, Jin AP (2006) Int J Electrochem Sci 1:317
26. Vadivel Murugan A, Reddy MV, Guy Campet, Vijayamohanan K (2007) J Electroanal Chem 6003:287
27. Iriyanma Y, Abe T, Inaba M, Ogumi Z (2000) Solid State Ionics 10:95
28. Yuan XX, Chao YJ, Ma ZF, Deng XY (2007) Electrochem Commun 9:2591
29. Wang Y, Cao GZ (2006) Electrochim Acta 51:4865
30. Reddy MV, Ting Y, Show CH, Shen ZX, Lim CT, Subba Rao GV, Chowdari BVR (2007) Adv Funct Mater 17:2792
31. Das B, Reddy MV, Krishnamoorthi C, Tripathy S, Mahendiran R, Subba Rao GV, Chowdari BVR (2009) Electrochim Acta 54:3360
32. Cao L, Xu F, Liang YY, Li HL (2004) Adv Mater 20:1853
33. Hu ZA, Xie YL, Wang YX, Mo LP, Yang YY, Zhang ZY (2009) J Mater Chem Phys 114:990
34. Yuan XX, Chao YJ, Ma ZF, Deng XY (2007) J Electrochem Commun 9:2591
35. Wagemaker M, Kearley GJ, Van Well AA, Mutka H, Mulder FM (2003) J Am Chem Soc 125:840
36. Wang YF, Wu MY, Zhang WF (2008) Electrochim Acta 53:7863
37. Huang H, Zhang WK, Gan XP, Wang C, Zhang L (2007) Mater Lett 61:296